Title
Continuous Measurement of Stress-Induced Travel-Time Variations at SAFOD

Journal
Seismological Research Letters, 90(1)

ISSN
0895-0695

Authors
Yang, Chenhao
Niu, Fenglin
Daley, Thomas M
et al.

Publication Date
2019

DOI
10.1785/0220180080

Peer reviewed

Continuous Measurement of Stress-Induced Travel-Time Variations at SAFOD

by Chenhao Yang, Fenglin Niu, Thomas M. Daley, and Taka'aki Taira

Chenhao Yang and Fenglin Niu: Department of Earth, Environmental, and Planetary Sciences Rice University 6100 Main Street Houston, Texas 77005 U.S.A. niu@rice.edu; Thomas M. Daley: Earth Science Division Lawrence Berkeley National Laboratory 1 Cyclotron Road Berkeley, California 94720 U.S.A.; Taka'aki Taira: Berkeley Seismological Laboratory University of California 219 McCone Hall Berkeley, California 94720 U.S.A.

ABSTRACT

In situ stress measurement at seismogenic depth is critically important for deciphering fault zone processes. In this study, we conducted a second active-source crosswell field experiment at the Parkfield San Andreas Fault Observatory at Depth (SAFOD) drill site to investigate the detectability of stress-induced seismic velocity changes at the top part of the seismogenic zone. We employed the same configuration of our previous experiments, which deployed a piezoelectric source and a three-component (3C) accelerometer at 1 km deep inside the pilot and main holes, respectively. We also added a hydrophone, which is attached to the source, to monitor the repeatability of the source waveforms. Over a 40-day recording period, we confirmed an ~0.04% travel-time variation in *S* wave and coda that roughly follows the fluctuation of barometric pressure. We attributed this correlation to stress sensitivity of seismic velocity and the stress sensitivity is estimated to be 2.0×10^{-7} Pa^{-1}, which is approximately two orders of magnitude higher than those measured in laboratory with dry rock samples, but is consistent with our previous results. Our results confirm the hypothesis that substantial cracks and/or pore spaces exist at seismogenic depths and thus may be used to monitor the subsurface stress field with active-source crosswell seismic.

INTRODUCTION

Earthquakes are caused by the sudden release of stresses along faults. Thus, the time-varying stress field at seismogenic depths is perhaps the most crucial parameter for understanding fault zone processes. Although recent studies suggest that stress release can manifest as a small or large earthquake (e.g., Lay and Kanamori, 2011), as aseismic slip (e.g., Niu *et al.*, 2003; Murray and Segall, 2005), or as nonvolcanic tremor (e.g., Nadeau and Dolenc, 2005), it is also found that many processes, such as fault interactions, can significantly affect the long-term stress build up described by plate tectonics (e.g., Freed and Lin, 2001; Xiong *et al.*, 2017). *In situ* measurement of the stress changes at seismogenic depths thus plays a critical role in deciphering fault zone processes, although the measurement itself is notoriously difficult.

It is well known from laboratory experiments that when crustal rocks are subjected to different levels of stress, their seismic velocity changes with the applied stress (e.g., Birch, 1960; Scholz, 1968; Nur and Simmons, 1969; Jones, 1983). Such a stress dependence of seismic velocity is attributed to the presence of microcracks within those rocks, and to the fact that the number of open microcracks and their stiffness can vary with the confining stress. The stress sensitivity, defined as $\eta = d\ln V/dP$ (Silver *et al.*, 2007), is found to be around 10^{-7} Pa^{-1} right below Earth's surface and decays rapidly to 10^{-9} Pa^{-1} at ~1 km depth (e.g., Birch, 1960; Nur and Simmons, 1969). Meanwhile, many field experiments also have been conducted to detect known stress variations, such as those related to the tidal stress, by measuring their induced seismic velocity changes, which is accomplished through shooting seismic waves repeatedly and measuring the delay times among different shots (e.g., De Fazio *et al.*, 1973; Reasenberg and Aki, 1974; Leary *et al.*, 1979). These early studies were generally not conclusive due to insufficient precision in the delay time measurements, probably caused by low-source repeatability.

Recent advances in control source and data acquisition techniques triggered new efforts to develop a seismic stress meter by utilizing the stress sensitivity of seismic velocity. Yamamura *et al.* (2003) conducted a field experiment in a vault near the coast of Miura Bay, Japan, using a highly repeatable piezoelectric source and found that the measured *P*-wave velocity responds regularly to the tidal stress changes. They obtained a stress sensitivity of 5×10^{-7} $Pa-^{1}$. Silver *et al.* (2007) also conducted a series of cross-well experiments to continuously measure *in situ* seismic velocity at two test sites: building 64 (B64) and Richmond field station (RFS) of the Lawrence Berkeley National Laboratory in California, from which they demonstrated that changes in seismic velocity induced by variations of barometric pressure are indeed observable at very shallow depth. The stress sensitivity is estimated to be $\sim10^{-6}$ Pa^{-1} and 10^{-7} Pa^{-1} at the B64 and RFS sites, respectively. These *in situ* estimates of the stress sensitivity are in good agreement with the laboratory results.

More recently, scientists from the China Earthquake Administration made large efforts to reinvent airgun as a highly repeatable and powerful source (e.g., Chen *et al.*, 2007; She *et al.*, 2018), a key component of the seismic stress monitoring system. Numerous tests with large volume airgun sources have been conducted inside natural and man-made lakes, rivers, and even boreholes across China. Several fixed airgun signal transmission stations have been built at different parts of Mainland China to monitor structural changes along active faults and dams (e.g., Wang *et al.*, 2018; Wei *et al.*, 2018).

Niu *et al.* (2008) conducted a continuous active-source crosswell experiment to measure seismic velocity changes at the Parkfield San Andreas Fault Observatory at Depth (SAFOD) drill site in California (Fig. 1). They deployed a piezoelectric source and a three-component (3C) accelerometer at ~1 km

deep inside the pilot and main holes, respectively. Over a two month period, they found a 0.3% change in the average *S*-wave velocity along a ~10 m baseline. The velocity change showed a good negative correlation with the barometric pressure, and the stress sensitivity is estimated to be 2.4×10^{-7} Pa^{-1}, which is much larger than those ($\sim10^{-9}$ Pa^{-1}) obtained in laboratory (e.g., Birch, 1960; Scholz, 1968; Nur and Simmons, 1969; Jones, 1983). They also detected two velocity drops associated with two earthquakes that are located a few fault length away from the instruments. In this study, we present the results from a similar experiment being conducted in early 2010. We added a hydrophone near the source in the pilot hole to monitor the stability of the source to ensure that changes measured from repeated seismic recordings are not due to changes in source wavelet. We confirmed an anticorrelation between the observed velocity changes and barometric pressure variations, and a high-stress sensitivity of 2.0×10^{-7} Pa^{-1}.

DATA AND ANALYSIS

We adopted the same techniques developed in Silver *et al.* (2007) and Niu *et al.* (2008) for experimental design, data acquisition, and analysis. Here, we review them briefly. More details can be found in Silver *et al.* (2007) and Niu *et al.* (2008).

Data Acquisition

We employed roughly the same data acquisition as Niu *et al.* (2008), which consisted a specially made source and a commercially available 3C accelerometer. The source includes nine half-cylinders of piezoelectric ceramic (lead zirconate titanate) wired for positive and negative voltage on the inner and outer surfaces and housed in an oil-filled cylindrical shell. We use a custom high voltage amplifier (HVA) to power the source, and employed a “Geode” recording system manufactured by Geometrics to digitize the waveform data. The HVA and Geode were placed inside an air-conditioned hut with very small temperature variations (<±1°C) to minimize thermally induced noise in the surface instruments (described in Silver *et al.*, 2007).

As part of the downhole instrument package of the SAFOD project, we installed the 3C accelerometer in the SAFOD main hole (Fig. 1) in September 2008. The instrument was installed at a depth of ~1 km below the surface. Because of a schedule conflict, we were unable to deploy the source to the pilot hole until November 2009. We also attached a hydrophone to the piezoelectric source to monitor potential changes in the source waveform. We did not have the hydrophone component in our previous deployment in 2005–2006 (Niu *et al.*, 2008). We had a severe crosstalk issue between our system and the U.S. Geological Survey seismometer at the bottom of the main borehole right after we installed the source. We were able to finally solve the crosstalk issue and started the recording on 11 February 2010. The sensor started deteriorating in late March and stopped completely on 2 April

2010, which we later found was caused by leakage of borehole fluid following corrosion of aluminum components of the accelerometer tool housing.

We employed roughly the same scheme of Niu *et al.* (2008) in acquiring the seismic data. We generated an ~2 V square wave with a period of 1 ms every 250 ms, which was boosted to ~1 kV by the HVA and sent to the piezoelectric source. We call these two signals the low-V and high-V, respectively. We used the low-V pulse to trigger the Geode to record 200 ms waveform data at a sampling rate of 48,000 samples per second for each shot record. The waveforms from each 100 shots were automatically stacked. We stacked and recorded a total of six channels of data, three from the 3C accelerometer, two for the source pulses before and after the amplification, and one from the hydrophone that was attached to the piezoelectric source. Figure 2 shows an example of the waveforms (Fig. 2a) recorded by the 3C accelerometer, as well as their amplitude spectra, which indicates the dominant energy is observed in the frequency range of 2–4 kHz (Fig. 2b). Figure 3a shows an example of the records of the hydrophone and outputs from the source pulse generator (low-V) and the HVA (high-V).

Delay Time Measurement and Error Estimations

Because of the processing time of the automatic stacking of the Geode, we generally obtained one short record every 25.67 s. Following Niu *et al.* (2008), we further manually stacked the records for another 100 times, which results in an approximately 1 shot record every 43 min. We employed these ~43min stacked records to conduct delay time analysis. Based on the frequency content of the accelerometer recordings shown in Figure 2b, we first filtered the data with a band-pass filter between 2 and 4 kHz. We then used a cross-correlation-based technique that is capable to measure the delay time with a subsample precision. More specifically, we first computed the cross-correlation function in the time domain and then fit it with a cosine function. We searched the largest sample point of the cross-correlation function, $cc(i_{max})$, and its two neighbor points $cc(i_{max-1})$ and $cc(i_{max+1})$. Cespedes *et al.* (1995) showed that the subsample shift is given by following expression:

$$\tau = -\tan^{-1}\left(\frac{cc(i_{max}-1)-cc(i_{max}+1)}{2cc(i_{max})\sin\alpha}\right)/\alpha, \qquad (1)$$

in which,

$$\alpha = \cos^{-1}\left(\frac{cc(i_{max}-1)+cc(i_{max}+1)}{2cc(i_{max})}\right). \qquad (2)$$

Silver *et al.* (2007) and Cheng *et al.* (2007) used different approaches to derive a low bound of the uncertainty in the delay time estimate (DTE)

$$\sigma_{\mathrm{DTE}} \geq \frac{1}{2\pi f_0 \times \mathrm{SNR}}, \qquad (3)$$

in which f_0 is the dominant frequency of the source pulse and SNR is the signal-to-noise ratio. Equation (3) indicates that the SNR is the only parameter that controls the precision in our DTE when the digitizing error is much less than the background noise. The precision is not controlled by the sampling rate of the digitizer and it is possible to obtain subsampling interval measurements of the time delay. As shown in Figure 2b, the dominant frequency of our data is between 2 and 4 kHz and the SNR measured from the three data channel is around 5000 for the 43-min stacked data. These values suggest that the best achievable precision in DTE is ~1×10−8 s or ~10 ns.

We assumed that the noise is random in the derivation of equation (3), the DTE precision, however, could also be affected by other nonrandom noises, such as changes in source waveform, errors in trigger timing and digitizer's clock. To estimate the potential changes in the square pulses input to the piezoelectric source, we measured delay time between each two consecutive samples, which roughly follows the Gaussian distribution with a standard variation of 3.1 and 1.1 ns for the low-V and high-V pulses, respectively (Fig. 3b). We also made the same DTE measurements with the waveform data recorded by the hydrophone, which is also shown in Figure 3b. The delay time also follows a Gaussian distribution with a standard variation of 1.1 ns. These values suggest that the source pulse generator, the HVA, and the piezoelectric source were very stable in the acquisition period. Silver *et al.* (2007) discussed the uncertainties in the triggering time, which is expected to be ~260 ns per trigger. Assuming the error of different triggers is uncorrelated and the error in the stacked data is smaller by a factor of $N^{1/2}$, we obtained an error of 2.6 ns for the 10,000-time stacked 43 min records.

Figure 4 shows the measured delay time between two consecutive recordings of the three data channels. We chose a time window from 9 to 30 ms, which comprises the *S* arrival and its coda, in computing the cross-correlation function. The long time window was chosen here to include as much of seismic energy as possible, because errors in the delay time measurement are inversely proportional to the signal strength, as shown in equation (3). Niu *et al.* (2008) employed two time windows, one short window including mostly the *S* wave and another long window that includes the major *S*-wave coda to measure delay times and found that the delay times measured from the long window are generally larger than those measured from the short window. The comparison of delay times measured at difference elapse time is known as coda-wave interferometry, which is a widely used technique to evaluate changes in the subsurface structure (Snieder *et al.*, 2002; Niu *et al.*, 2003). The *S* wave in this acquisition is less developed and the time delay with the short window is less stable, therefore, we used the measurements from the long window. This is also the reason

that we did not choose the *P*-wave window in the delay time measurement, as the recorded *P*-wave energy is generally small (Fig. 2a). The measured delay times of channel 1, 2, and 3 also exhibit a Gaussian distribution with a standard variation of 357.9, 103.3, and 228.2 ns (or ~0.36, ~0.10, and ~0.23 μs), respectively. In general, these values are much larger than the theoretical low bound in equation (3), suggesting that the measured delay times between the consecutive samples shown in Figure 4 are not entirely caused by random noise. In fact, we expect that there is a contribution from actual velocity perturbations of the subsurface structure.

RESULTS AND DISCUSSION

Although we started the data acquisition on 11 February 2010, we had several instrumental issues in the first few days, which led to data gaps in this period. In the data analysis, we chose a total of 1350 43 min records that covered the period from 19 February to 30 March 2010. We first stacked all the records to create a reference trace. We then applied the cross-correlation-based DTE technique to measure the delay times of the *S* wave plus its coda up to 30 ms with respect to the reference trace. The measured delay times from the three data channels are shown in Figure 5a. In general, the results measured from the three channels are in good agreement with the others. There are several spikes in the measured delay times of channel 1 (Fig. 5a), suggesting that it is noisier than the other two channels. The histograms shown in Figure 4 also indicate that channel 1 has a measurement error larger than the other two channels.

Over the 40 day period, the largest perturbation of the measured delay time occurred in the first 10 day period, in which the delay time dropped rapidly from ~3 to ~−5 μs and then recovered quickly by ~7 μs. This period also witnessed the largest fluctuation in the record of barometric pressure (Fig. 5b). The computed cross-correlation function of the two records shows a negative peak at nearly zero lag time (Fig. 5b, inset), suggesting that the largest perturbation in the delay time record is likely caused by the large fluctuation of barometric pressure. The total travel-time variation observed here is around 8 μs, which converts to a velocity perturbation of $|\frac{\delta v}{v}| = |\frac{\delta t}{t}| = 4\times10^{-4}$, assuming an average travel time of 20 ms for the *S*-plus coda waves. Meanwhile, the barometric pressure change at surface in the same period is ~2000 Pa. As a weather system usually covers an area much larger than 1 km, it is reasonable to employ a half-space model with uniform loading at the surface to compute the subsurface stress field. Under this assumption, we can directly translate the barometric pressure change measured at surface to the stress perturbation at 1 km depth. This leads to an estimate of the stress sensitivity to be approximately 2.0×10^{-7} Pa^{-1}. Nur and Simmons (1969) measured the stress sensitivity of the *P*- and *S*-wave velocities of dry and wet rock samples in the lab and found that the velocity–stress sensitivity drops from 10^{-7} Pa^{-1} at surface to 10^{-9} Pa^{-1} at 1 km depth. Thus, our observation here is approximately two orders of magnitude larger

than the laboratory measurements. The velocity–stress sensitivity of rocks is highly sensitive to crack density and presence of fluids; therefore, our measurement here might suggest that rocks the SADOF site have higher crack density than sample rocks used in the laboratory study (Nur and Simmons, 1969). In fact, the observed value here falls in the range of field observations, 10^{-6} to 10^{-9} Pa^{-1}, reported by many past studies (Yamamura *et al.*, 2003, and the references; Silver *et al.*, 2007; Niu *et al.*, 2008). Stress-induced fluid redistribution might also have raised the *S*-wave stress sensitivity here, as the shear modulus is highly sensitive to the presence of fluids.

Other driving forces could be used to estimate stress sensitivity, such as Earth tides or thermoelastic stress change. Niu *et al.* (2008) computed the stress variations associated with solid Earth tides at the SAFOD drill site and found that the amplitude is around ~200 Pa, which is about 10 times smaller than the barometric pressure changes. Using the above stress sensitivity, the Earth-tide-induced travel-time changes are on the order of 0.8 μs, which is barely above the measurement error and is thus more difficult to be observed robustly. Ben-Zion and Allam (2013) computed thermoelastic stress changes at Parkfield and obtained an areal strain of $\sim 1.3\times10^{-7}$ at 1 km depth, which converts to ~4000 Pa assuming a bulk modulus of 30 GPa. They also found the thermal strain has a dominant period of one year and is delayed by ~45 days from the source temperature field. Because we have only 40 days of data, it is almost impossible to observe this long annual circle. We are therefore left with barometric pressure change as our driving force for estimating the stress sensitivity at our recording depth. We noticed that the negative correlation between the delay time and barometric pressure becomes elusive in the middle part of the records, which suggests the processes associated with delay time changes are likely more complicated than simple elastic responses to barometric pressure stress changes.

We also computed the coseismic stress changes associated with local earthquakes that occurred in the observed period. There are a total of 71 earthquakes in the Northern California Seismic Network (NCSN) catalog (Northern California Earthquake Data Center [NCEDC], 2014), among which one **M** 3.4 earthquake occurred at 22:44:49.39 UTC on 25 March 2010 (open square in Fig. 1). This earthquake has a focal depth of ~9.2 km, much deeper than the **M** 3 event (3.9 km deep) observed by Niu *et al.* (2008) (hereafter referred to as 2005 **M** 3 event). Therefore, the calculated stress change at our sensor site, for this earthquake, is only 115 Pa assuming a coseismic stress drop of 5 MPa at the source, which is approximately 27% of that of the 2005 **M** 3 event. Although all the three channels showed an increase of travel time several hours before the earthquake (Fig. 6), the data appeared to be much noisier in this time period. We noticed that the maximum amplitude of the individual raw records exhibited large variations (top panels in Figs. 6a–c) and the cross-correlation coefficient also showed a

significant drop (bottom panels). We speculate that the accelerometer might have started deteriorating due to fluid leakage (the shaded time period in Fig. 6). Therefore, we believe it is inconclusive that the rise in travel time is related to the earthquake.

CONCLUSIONS

We conducted a second cross-well experiment at the Parkfield SAFOD drill site in 2010 to confirm the feasibility, and repeatability, of monitoring stress transients at seismogenic depth with active-source seismic data. Over an ~40 day period, we observed an ~0.04% variation in the average *S*-wave velocity around the pilot and main holes at ~1 km depth, which we interpret to be caused by changes in barometric pressures as the observed velocity perturbation appears to correlate negatively with the barometric pressure. From this correlation, we estimated the velocity–stress sensitivity is $\sim 2.0\times10^{-7}$ Pa^{-1}, which is significantly larger than those measured from dry rock samples in laboratory, but is roughly the same as we obtained in our first experiment (Niu *et al.*, 2008). Our results thus confirm the hypothesis that substantial cracks and/or pore spaces exist at seismogenic depths and may thus be used to monitor the subsurface stress field. We also observed a gradual rise of *S*-wave travel time slightly before an **M** 3.4 earthquake, which occurred about 10 km away from the experiment site approximately one week before the failure of the accelerometer in the main hole. However, we also found that our recordings were much noisier during this period, which we speculate is from a deteriorating sensor, and consequently the *S*-wave velocity drop before the seismic event is considered inconclusive. In addition to barometric pressure, thermal stress changes could be significant and used as another calibrating source. Our results confirm the sensitivity and repeatability of long-term active-source crosswell seismic velocity monitoring for stress change at depth.

DATA AND RESOURCES

The earthquake catalog was downloaded from the Data Center of the Northern California Seismic Network (NCSN) (Northern California Earthquake Data Center [NCEDC], 2014). The waveforms used in this study were collected as part of the San Andreas Fault Observatory at Depth (SAFOD) cross-well active-source monitoring experiment with a Program for Array Seismic Studies of the Continental Lithosphere (PASSCAL) owned Geode. Data are available from the Incorporated Research Institutions for Seismology (IRIS) Data Management Center at www.iris.edu (last accessed August 2011).

ACKNOWLEDGMENTS

The authors would like to thank all the people at Lawrence Berkeley National Laboratory (LBNL) Geoscience Measurement Facility (GMF) who helped us in preparing, testing, and installing the instruments. The authors also thank *SRL* Editor-in-Chief Zhigang Peng and three anonymous reviewers for their

constructive comments and suggestions, which significantly improved the quality of this article. This work was supported by National Science Foundation (NSF) Grant Numbers EAR-1251667 (C. Y., F. N., and T. D.) and EAR-1251998 (T. T.). Work at LBNL is supported under Contract Number DE-AC02-05CH11231.

REFERENCES

Ben-Zion, Y., and A. A. Allam (2013). Seasonal thermoelastic strain and postseismic effects in Parkfield borehole dilatometers, Earth Planet. Sci. Lett. 379, 120–126.

Birch, F. (1960). The velocity of compressional waves in rocks to 10 kilobars, part 1, J. Geophys. Res. 65, 1083–1102.

Cespedes, I., Y. Huang, J. Ophir, and S. Spratt (1995). Methods for estimation of sub-sample time delays of digitized echo signals, Ultrason. Imag. 17, 142–171.

Chen, Y., X. Zhang, X. Qiu, H. Ge, B. Liu, and B. Wang (2007). A new method to generate seismic wave on the land, Chin. Sci. Bull. 52, no. 11, 1317–1321, doi: 10.3321/j.issn:0023-074X.2007.11.017 (in Chinese).

Cheng, X., F. Niu, P. G. Silver, S. Horiuchi, K. Takai, Y. Iio, and H. Ito (2007). Similar microearthquakes observed in western Nagano, Japan, and implications for rupture mechanics, J. Geophys. Res. 112, no. B04306, doi: 10.1029/2006JB004416.

De Fazio, T. L., K. Aki, and J. Alba (1973). Solid earth tide and observed change in the in situ seismic velocity, J. Geophys. Res. 78, 1319–1322.

Freed, A. M., and J. Lin (2001). Delayed triggering of the 1999 Hector Mine earthquake by viscoelastic stress transfer, Nature 411, 180–183.

Jones, T. D. (1983). Wave propagation in porous rock and models for crustal structure, Ph.D. Thesis, Stanford University, Stanford, California, 223 pp.

Lay, T., and H. Kanamori (2011). Insights from the great 2011 Japan earthquake, Phys. Today 64, 33–39.

Leary, P. C., P. E. Malin, R. A. Phinny, T. Brocher, and R. Voncolln (1979). Systematic monitoring of millisecond travel time variations near Palmdale, California, J. Geophys. Res. 84, 659–666.

Murray, J. R., and P. Segall (2005). Spatiotemporal evolution of a transient slip event on the San Andreas fault near Parkfield, California, J. Geophys. Res. 110, no. B09407, doi: 10.1029/2005JB003651.

Nadeau, R. M., and D. Dolenc (2005). Nonvolcanic tremors deep beneath the San Andreas fault, Science 307, 389.

Niu, F., P. G. Silver, T. Daley, X. Cheng, and E. Majer (2008). Preseismic velocity changes observed from active source monitoring at the Parkfield SAFOD drill site, Nature 454, 204–208, doi: 10.1038/ nature07111.

Niu, F, P. G. Silver, R. M. Nadeau, and T. V. McEvilly (2003). Migration of seismic scatterers associated with the 1993 Parkfield aseismic transient event, Nature 426, 544–548, doi: 10.1038/nature02151.

Northern California Earthquake Data Center (NCEDC) (2014). Northern California Earthquake Data Center, UC Berkeley Seismological Laboratory, Dataset, doi: 10.7932/NCEDC.

Nur, A., and G. Simmons (1969). The effect of saturation on velocity in low porosity rocks, Earth Planet. Sci. Lett. 7, 183–193.

Reasenberg, P., and K. Aki (1974). A precise, continuous measurement of seismic velocity for monitoring in situ stress, J. Geophys. Res. 79, 399–406.

Scholz, C. H. (1968). Microfracturing and the inelastic deformation of rock I: Compression, J. Geophys. Res. 73, 1417–1432.

She, Y., H. Yao, Q. Zhai, F. Wang, and X. Tian (2018). Shallow crustal structure of the middle-lower Yangtze River region in eastern China from surface-wave tomography of a large volume airgun shot experiment, Seismol. Res. Lett. 89, no. 3, 1003–1013, doi: 10.1785/0220170232.

Silver, P. G., T. M. Daley, F. Niu, and E. L. Majer (2007). Active source monitoring of cross-well seismic travel time for stress-induced changes, Bull. Seismol. Soc. Am. 97, 281–293.

Snieder, R., A. Gret, H. Douma, and J. Scales (2002). Coda wave interferometry for estimating nonlinear behavior in seismic velocity, Science 295, 2253–2255.

Wang, B., X. Tian, Y. Zhang, Y. Li,W. Yang, B. Zhang,W. Wang, J. Yang, and X. Li (2018). Seismic signature of untuned large-volume airgun array fired in a water reservoir, Seismol. Res. Lett. 89, no. 3, 983–991, doi: 10.1785/0220180007.

Wei, C., M. Qin, Y. Zhang, R. Zou, L. Wang, X. Guo, X. Liu, Y. Wang, and D. Sun (2018). Airgun excitation experiments at different placement depths in the Qilian Mountain of Gansu Province, China, Seismol. Res. Lett. 89, no. 3, 974–982, doi: 10.1785/0220170253.

Xiong, X., B. Shan,Y. Zhou, S. Wei, Y. Li, R. Wang, and Y. Zheng (2017). Coulomb stress transfer and accumulation on the Sagaing Fault, Myanmar, over the past 110 years and its implications for seismic hazard, Geophys. Res. Lett. 44, 4781–4789.

Yamamura, K., O. Sano, H. Utada, Y. Takei, S. Nakao, and Y. Fukao (2003). Long-term observation of in situ seismic velocity and attenuation, J. Geophys. Res. 108, doi: 10.1029/2002JB002005.

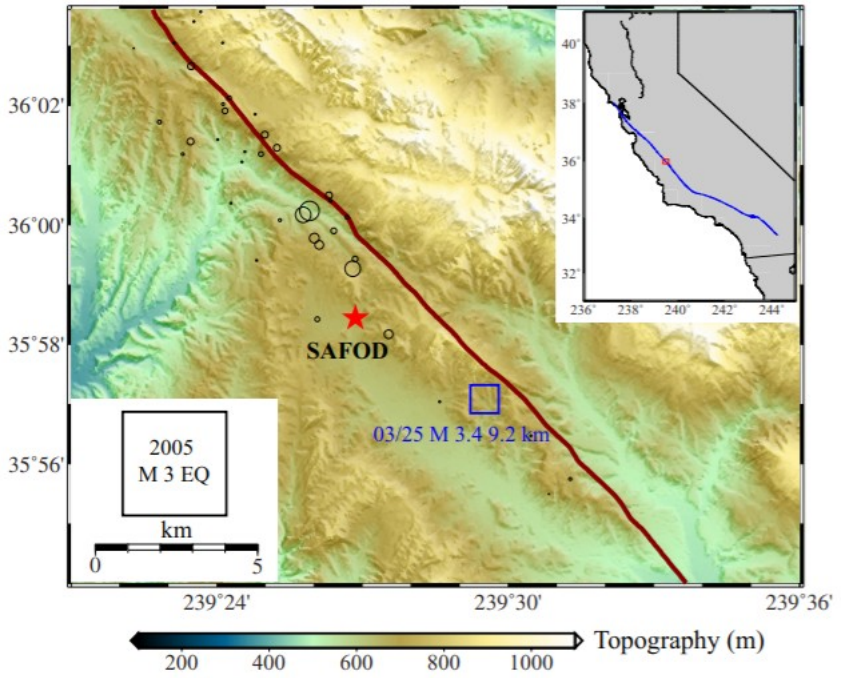

▲ **Figure 1.** Topography map showing the surface trace of the San Andreas fault (thick line) and the San Andreas Fault Observatory at Depth (SAFOD) drill site (star). Earthquakes occurred during the experiment period are shown by circles. The open square indicates the **M** 3.4 earthquake that occurred on 25 March 2010 The size of the square is scaled by the calculated coseismic stress change with respect to the stress drop of the 2005 **M** 3 earthquake (open square in the legend) discussed in Niu *et al.* (2008). (Upper right inset) Part of the United States and Mexico. The study area and the San Andreas fault are indicated by the square and thick solid line, respectively. The color version of this figure is available only in the electronic edition.

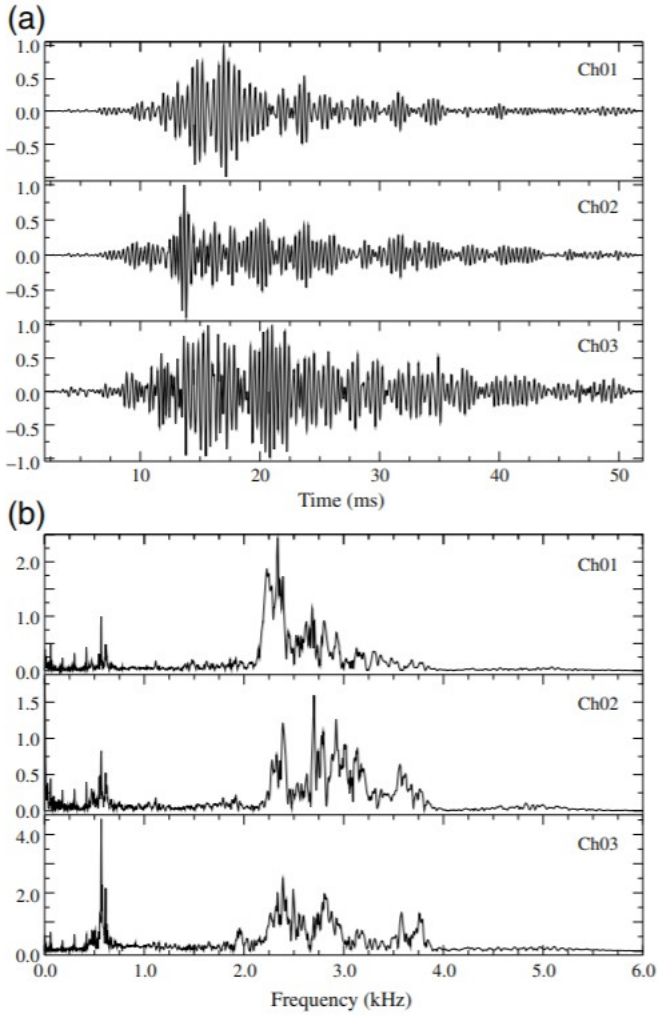

▲ **Figure 2.** (a) An example of the first ~50 ms of the raw three-component (3C) acceleration records and (b) their corresponding amplitude spectra.

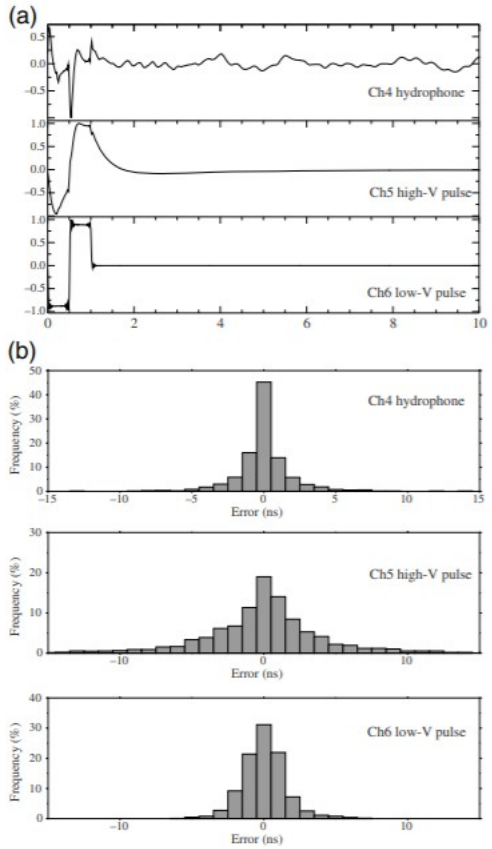

▲ **Figure 3.** (a) An example of the waveform records of the three auxiliary channels, which are hydrophone (velocity), high-V pulse, and low-V pulse from the top to the bottom. Only the first 10 ms of the records are shown here. (b) Histogram of the measured delay times between two consecutive 43 min records of the three auxiliary channels. The standard deviations of the delay times, which represent the upper bands of the potential variations in the source pulses at different levels, are less than 5 ns, suggesting that the source possessed an excellent capability in generating highly repeatable pulses.

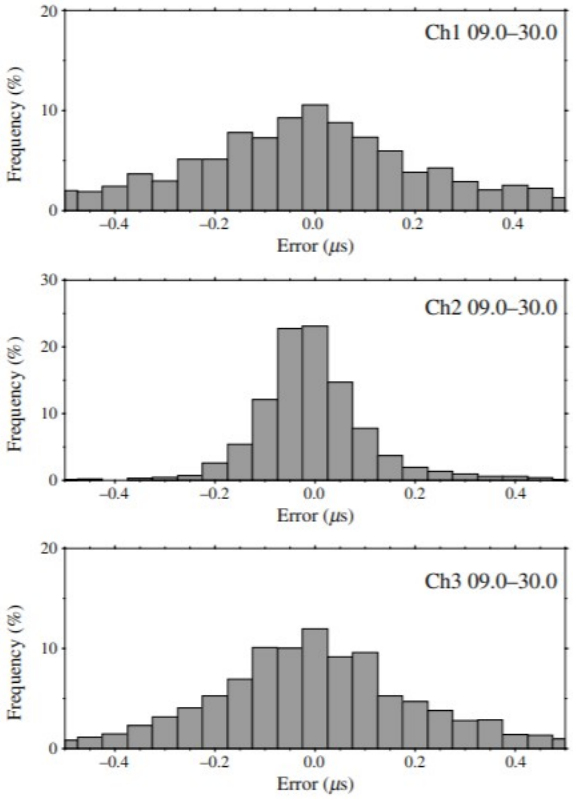

▲ **Figure 4.** Histograms of the measured delay times between two consecutive 43 min records of the three data channels. A time window of 9–30 ms is used in the measurements. The estimated delay times follow Gaussian distributions with standard deviations of a few tenths of μs, which can be considered as the upper bands of the potential uncertainties in the delay time estimate (DTE).

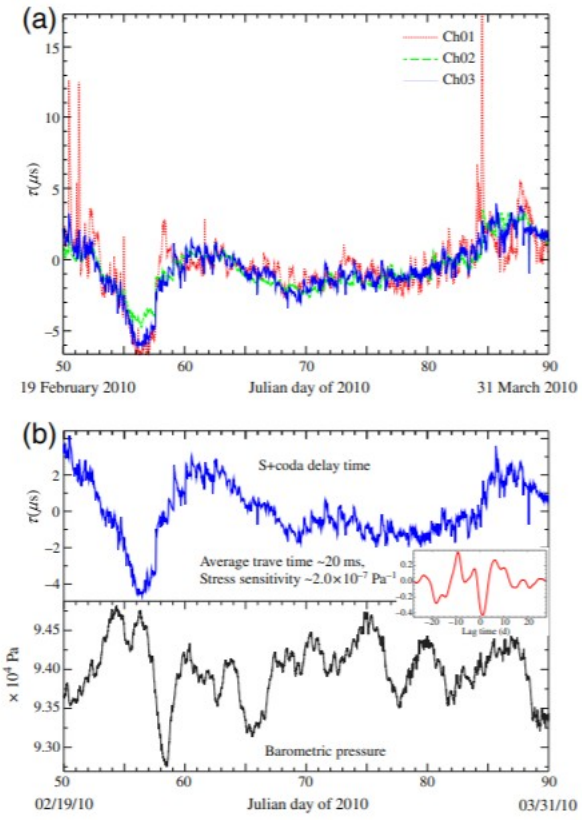

▲ **Figure 5.** (a) Delay times estimated from the *S*-wave arrival plus the coda recorded on the three components are shown together for comparison. In general, they agree well with each other except for the spikes on the first channel (dotted line). (b) Delay time estimated from the *S*-wave arrival plus the coda recorded by channel 3 is shown together with the barometric pressure. The two curves exhibit a roughly negative correlation. (Inset) The cross-correlation function computed from the first 28 days of the two records. The color version of this figure is available only in the electronic edition.

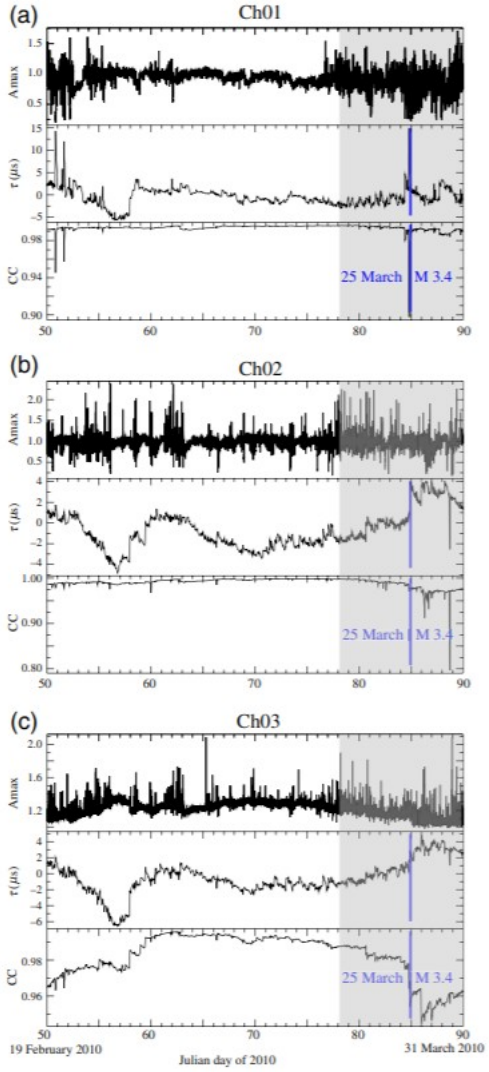

▲ **Figure 6.** (a) The maximum amplitude of individual records, the measured delay time, and the cross correlation between the 43 min records and the reference trace of channel 1 are shown from the top to the bottom. The thick vertical lines indicate the time when the **M** 3.4 earthquake occurred. The shaded area represents the final stage of the recording that is featured by large amplitude perturbations and low-correlation coefficients, which may suggests that the 3C accelerometer is deteriorating before its final collapse on 2 April. (b,c) Similar to (a) except for channels 2 and 3, respectively. The color version of this figure is available only in the electronic edition.